SAGE-Hindawi Access to Research
Enzyme Research
Volume 2011, Article ID 307464, 7 pages
doi:10.4061/2011/307464

Research Article

Towards Al^{3+}-Induced Manganese-Containing Superoxide Dismutase Inactivation and Conformational Changes: An Integrating Study with Docking Simulations

Jiang-Liu Yang,[1] Shang-Jun Yin,[2] Yue-Xiu Si,[2] Zhi-Rong Lü,[3,4] Xiangrong Shao,[4] Daeui Park,[5] Hae Young Chung,[5] Hai-Meng Zhou,[3,4] Guo-Ying Qian,[2] and Zi-Ping Zhang[1]

[1] *School of Life Science, Ningxia University, Yinchuan 750021, China*
[2] *College of Biological and Environmental Sciences, Zhejiang Wanli University, Ningbo 315100, China*
[3] *School of Life Sciences, Tsinghua University, Beijing 100084, China*
[4] *Zhejiang Provincial Key Laboratory of Applied Enzymology, Yangtze Delta Region Institute of Tsinghua University, Jiaxing 314006, China*
[5] *Molecular Inflammation Research Center for Aging Intervention (MRCA), College of Pharmacy, Pusan National University, Busan 609-735, Republic of Korea*

Correspondence should be addressed to Guo-Ying Qian, qianguoying_wanli@hotmail.com and Zi-Ping Zhang, zpzhang@nxu.edu.cn

Received 8 March 2011; Accepted 29 March 2011

Academic Editor: Yong-Doo Park

Superoxide dismutase (SOD, EC 1.15.1.1) plays an important antioxidant defense role in skins exposed to oxygen. We studied the inhibitory effects of Al^{3+} on the activity and conformation of manganese-containing SOD (Mn-SOD). Mn-SOD was significantly inactivated by Al^{3+} in a dose-dependent manner. The kinetic studies showed that Al^{3+} inactivated Mn-SOD follows the first-order reaction. Al^{3+} increased the degree of secondary structure of Mn-SOD and also disrupted the tertiary structure of Mn-SOD, which directly resulted in enzyme inactivation. We further simulated the docking between Mn-SOD and Al^{3+} (binding energy for Dock 6.3: −14.07 kcal/mol) and suggested that ASP152 and GLU157 residues were predicted to interact with Al^{3+}, which are not located in the Mn-contained active site. Our results provide insight into the inactivation of Mn-SOD during unfolding in the presence of Al^{3+} and allow us to describe a ligand binding via inhibition kinetics combined with the computational prediction.

1. Introduction

Superoxide dismutases (SOD, EC 1.15.1.1) are a class of enzymes that catalyze the dismutation of superoxide into oxygen and hydrogen peroxide [1–3]. They play an important antioxidant defense role in skins exposed to oxygen. In this regard, for the treatment of systemic inflammatory diseases including skin ulcer lesions, the topical application of free Mn-SOD or Cu, Zn-SOD extracted from bovine, bacterial, and other species was dramatically effective in skin lesions [4]. It has been reported that significant increase in the levels of SOD occurs in vitiligo patients due to the increased oxidative stress [5]. The involvement of oxidative stress in chronic idiopathic urticaria associated with SOD was also reported [6]: the activity of SOD was markedly increased in lesional skin as compared with skin of healthy subjects, indicating that oxidative stress is crucially involved in chronic idiopathic urticaria and suggesting that oxidative stress is secondary to the development of inflammation. The earlier reports [7, 8] suggested that the activity of activator protein-1, which is associated with tumor promotion, was reduced in Mn-SOD transgenic mice overexpressing Mn-SOD in the skin, suggesting that Mn-SOD reduced tumor incidence by suppressing activator protein-1 activation.

The mechanism of Mn-SOD catalysis is very important, and the mechanism therefore needs to be investigated from different sources using various kinetic methods. The information regarding the tertiary structure and the structural integrity of the active site of Mn-SOD is little known and in this regard, investigation on structure-function relationships

in this enzyme including docking of a ligand is important. In this study, we applied Al^{3+} to understand Mn-SOD structural changes and inhibition mechanisms. As a result, we proposed an inhibitory effect of Al^{3+} on Mn-SOD and suggest the mechanisms of combination between inhibition kinetics and computational prediction to depict the Al^{3+} action in the catalysis of Mn-SOD.

2. Materials and Methods

2.1. Materials. Aluminum chloride crystal ($AlCl_3 \cdot 6H_20$), Pyrogallol, and ANS were purchased from Sigma-Aldrich (USA). EDTA and Tris were from Fluka (Switzerland). The crude form of Mn-SOD (from *Thermus thermophilus*) was purchased from BioTech Company (China). We further purified Mn-SOD using the ÄKTAFPLC system (GE Healthcare, USA); a single band was obtained on both SDS-PAGE and native nonreducing PAGE gels. All other reagents used were local products of analytical grade. 10 mM Tris-HCl buffer (pH 8.2) was used during preparing all samples in this study.

2.2. Mn-SOD Assay. The assay for Mn-SOD was performed spectrophotometrically [9]. The activity of SOD was calculated according to the procedures of pyrogallol's autoxidation, which could be monitored by the change in absorbance at 325 nm per min. Reactions were performed in a typical reaction volume of 1 mL to which 10 μL of enzyme solution was added to measure Mn-SOD activity. The activity and absorption were measured with a Perkin Elmer Lambda Bio U/V spectrophotometer.

2.3. Circular Dichroism (CD) Spectroscopy. Far-UV CD spectra of Mn-SOD at different Al^{3+} concentrations were recorded on a Jasco J-810 Spectropolarimeter in the region of 190–250 nm at room temperature. The sample cell path length was 0.1 cm. CD measurements were carried out according to the provider's instructions. The final spectrum was obtained on the average of three scans. Blanks were collected and subtracted from the appropriate samples in data processing.

2.4. Intrinsic and ANS-Binding Fluorescence Measurements. Mn-SOD was denatured by incubation in 10 mM Tris-HCl (pH 8.2) containing various concentrations of Al^{3+} for 3 h, 25°C. The fluorescence emission spectra were measured with a Jasco FP750 spectrofluorometer with the use of a 1 cm path-length cuvette. An excitation wavelength of 280 nm was used for the tryptophan fluorescence measurements, and the emission wavelength ranged between 300 and 410 nm. The changes of the ANS-binding fluorescence intensity for Mn-SOD were studied by labeling with 40 μM ANS for 30 min prior to measurement. An excitation wavelength of 380 nm was used for the ANS-binding fluorescence, and the emission wavelength ranged from 400 to 650 nm.

2.5. Determination of the Binding Constant and the Number of Binding Sites. According to a previous report [10], when small molecules are bound to equivalent sites on a macromolecule, the equilibrium between free and bound molecules are given by the following equation to evaluate the binding constant (K) and number of binding sites (n):

$$\frac{F_0}{F_0 - F} = \frac{1}{n} + \frac{1}{K}\frac{1}{[Q]}, \tag{1}$$

where F_0 and F are the relative steady-state fluorescence intensities in the absence and presence of quencher, respectively. $[Q]$ is the quencher (Al^{3+}) concentration. The values for K and n can be derived from the intercept and slope of a plot based on (1).

2.6. In Silico Docking of Mn-SOD and Al^{3+}. The known 3D structure of Mn-SOD was obtained from PDB data base (ID: 3MDS). Among the many tools available for *in silico* protein-ligand docking, DOCK6.3 was applied because of its automated docking capability. The program performed ligand docking using a set of predefined 3D grids of the target protein and used a systemic search technique [11]. The original structure of Al^{3+} was derived from the PubChem database (Compound ID: 104727, http://www.pubchem.org/). To prepare for the docking procedure, the following steps were taken: (1) conversion of 2D structures to 3D structures, (2) calculation of charges, (3) addition of hydrogen atoms, and (4) location of pockets. For these steps, we used the fconverter program of the J-Chem package (http://www.chemaxon.com/) and OpenBabel (http://openbabel.org/).

3. Results

3.1. Effect of Al^{3+} on the Activity of Mn-SOD: Inactivation Kinetics. We assayed Mn-SOD at the equilibrium and the kinetic states in the presence of Al^{3+}. Mn-SOD was significantly inactivated by Al^{3+} with a dose-dependent manner (Figure 1). When the Al^{3+} concentration was increased to 0.8 mM, the activity of Mn-SOD was completely abolished. The IC_{50} value was measured as 0.19 mM ($n = 2$).

To evaluate the inactivation kinetics and rate constants, time interval measurements were performed. The different time courses of Mn-SOD in the presence of 0.2, 0.3, and 0.4 mM Al^{3+}, respectively, were recorded (Figure 2(a)). The enzyme activity was gradually decreased with time intervals and this implied that Al^{3+} may induce Mn-SOD tertiary structural change due to the fact that the activity of Mn-SOD was synchronized with the conformational changes. The microscopic inactivation rates constants (k_a) were properly calculated from the semilogarithmic plots (Figure 2(b)) where the reactions were plotting as two-phasic courses (fast, k_1 and slow, k_2). The rate constants for 0.2, 0.3, and 0.4 mM Al^{3+} were obtained as $k_1 = 7.39$, 7.83, and $13.3 \times 10^{-3}\,s^{-1}$, respectively, and $k_2 = 0.58$, 1.25, and $1.73 \times 10^{-3}\,s^{-1}$, respectively. These results suggested that the Mn-SOD inactivation by Al^{3+} followed the first-order kinetic process, and the enhancing Al^{3+} concentration could promote the inactivation rate.

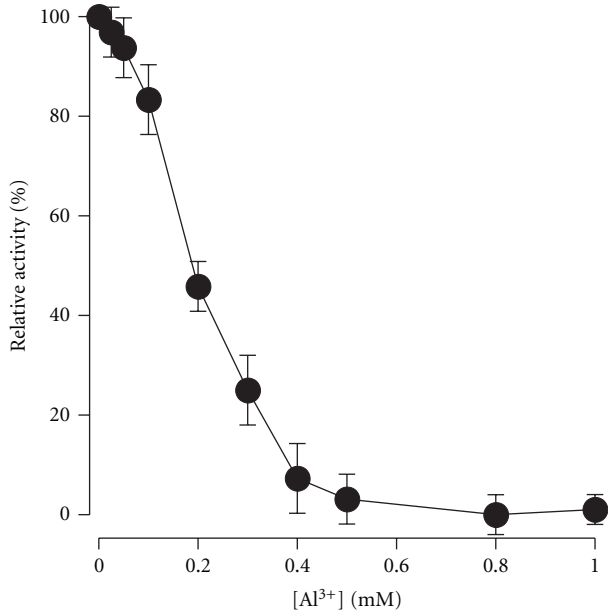

Figure 1: Inactivation of Mn-SOD in the presence of Al^{3+}. Data and bars are presented as means ($n = 2$). Mn-SOD was incubated with various concentrations of Al^{3+} for 3 h, and then added to the assay system in the presence of the corresponding concentrations of Al^{3+}. The final concentration of Mn-SOD was 1.25 μM.

3.2. Al^{3+}-Induced Secondary Structural Changes of Mn-SOD Measured by CD. To compare the enzyme activity changes with the secondary structural changes, we performed the Far-UV circular dichroism (CD) spectroscopy. As the concentration of Al^{3+}increased, the overall amount of secondary structure decreased gradually in a dose-dependent manner: specifically, the measurements for both 208 and 222 nm indicated that overall helical contents were decreased with increasing Al^{3+} concentration (Figure 3). Interestingly, the overall secondary structure of Mn-SOD was mostly sustained at lower than 0.3 mM Al^{3+} but the activity was drastically abolished by Al^{3+} in this range as shown in Figure 1.

3.3. Effect of Al^{3+} on the Tertiary Structure of Mn-SOD: Spectrofluorimetry Studies. Next, tertiary structural changes of Mn-SOD in the presence of Al^{3+} were also measured by intrinsic and ANS-binding fluorescences measurements. The intrinsic fluorescence changes showed that Al^{3+}might induce the unfolding of Mn-SOD which was monitored by the decrease of intrinsic fluorescence spectra (Figure 4). Based on the quenching effect of $Al^{3+}$and (1), we deduced a double reciprocal plot revealing a linear relationship (Figure 5). From this data, we calculated the binding constant as $K = 5.4 \pm 0.8 \times 10^3\ M^{-1}$ and the binding number as $n = 1.5 \pm 0.3$ according to plotting results and (1). These results revealed that Al^{3+} has a strong binding affinity for tyrosinase in the absence of substrate and that there are one or two possible binding sites.

The kinetics of Mn-SOD unfolding was also monitored (Figure 6(a)). The data of the semilogarithmic plots showed that the unfolding process also followed the first-order

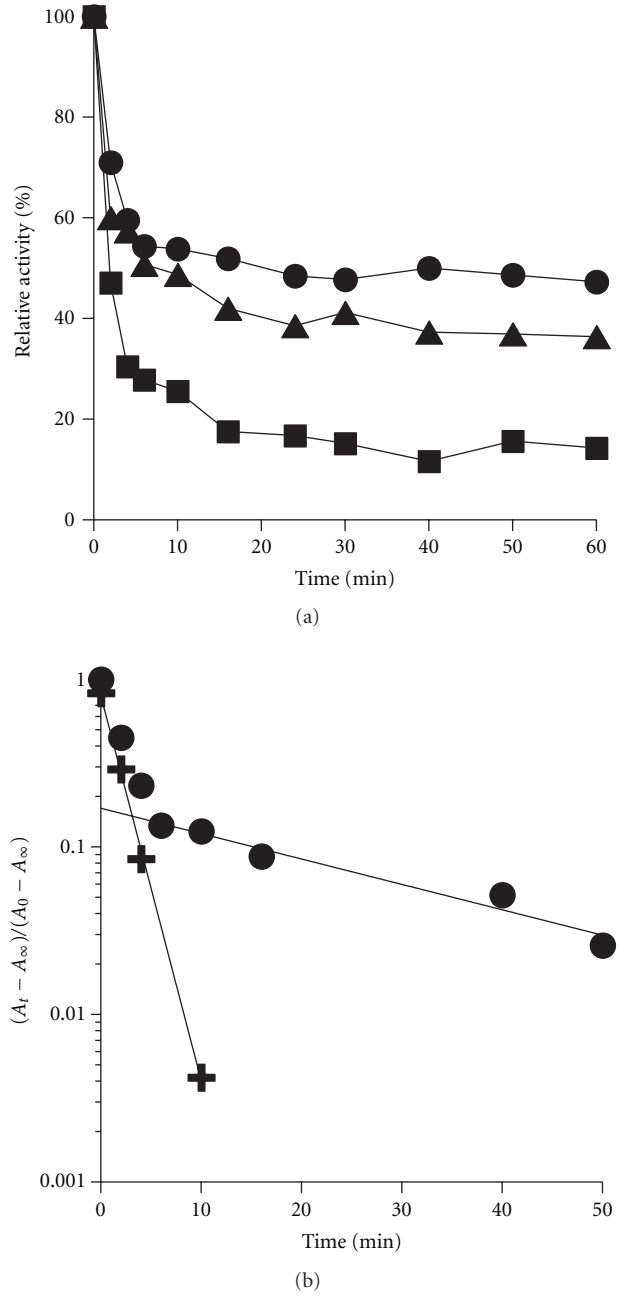

Figure 2: Inactivation kinetics of Mn-SOD in the presence of Al^{3+}. (a) The Al^{3+} concentrations were 0.2 (•), 0.3 (▲), and 0.4 mM (■), respectively. The reaction occurred at 25°C. The final concentration of Mn-SOD was 1.25 μM. (b) The semilogarithmic plot. The Al^{3+} concentration was 0.2 mM. (•) Experimental points. (+) Points obtained by subtracting the contribution of the slow phase from the data in the curve (- - -).

kinetics where the reactions were plotting as two-phasic courses (fast, ku_1 and slow, ku_2). The rates constants were calculated as $ku_1 = 2.89$ and $ku_2 = 0.21 \times 10^{-3}\ s^{-1}$ (Figure 6(b)). These results indicated that unfolding process of Mn-SOD was synchronized with the activity inactivation with the same order reaction, which was comparative to the results in Figure 2.

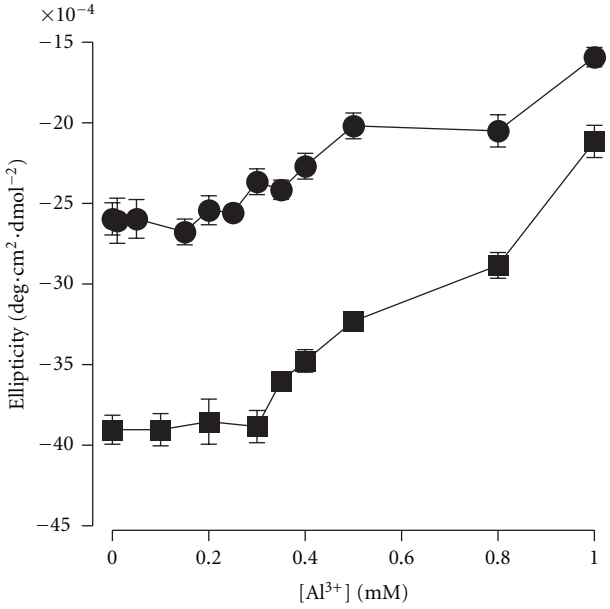

Figure 3: Far-ultraviolet CD spectra of Mn-SOD in the presence of different Al^{3+} concentrations. (a) Mn-SOD was incubated with Al^{3+} solutions for 3 h before measurement at 25°C. Blanks were collected and subtracted from the sample spectra in data processing. (b) CD spectra changes of Mn-SOD at 208 (•) and 222 (■) nm. Data indicate mean values ($n = 2$). The final Mn-SOD concentration was 20 μM.

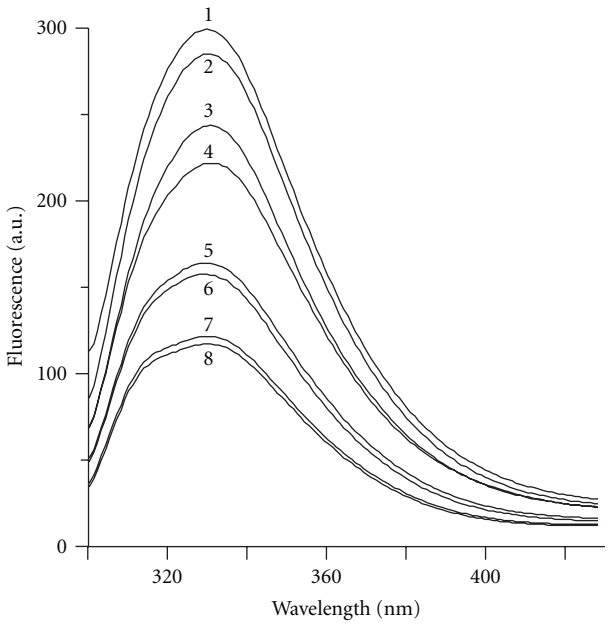

Figure 4: Intrinsic fluorescence changes of Mn-SOD by Al^{3+}. Intrinsic fluorescence spectra changes. Mn-SOD was incubated with Al^{3+} for 3 h before being measured. The final Mn-SOD concentration was 1.6 μM. Curves from 1 to 8 represent 0, 0.01, 0.05, 0.1, 0.2, 0.3, 0.4, and 0.5 Al^{3+} mM, respectively.

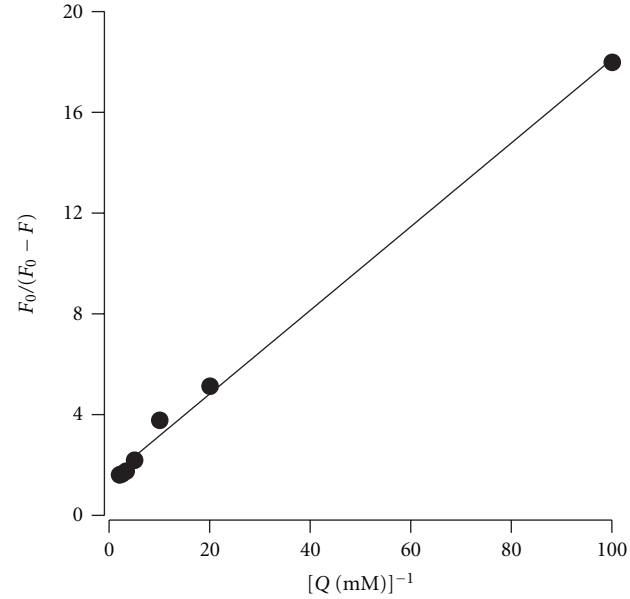

Figure 5: Double reciprocal plot of $F_0/(F_0 - F)$ versus $[Q]^{-1} \cdot F0$, native maximum fluorescence intensity; F: maximum fluorescence intensity of sample; Q: quencher Al^{3+}.

In the next step, we monitored the hydrophobicity changes of Mn-SOD in the presence of Al^{3+}. The ANS-fluorescence intensities were changed by overall range of Al^{3+} concentrations (Figure 7), indicating that hydrophobic surfaces of Mn-SOD were exposed during Al^{3+}-mediated unfolding. In general, ANS dye can bind to hydrophobic amino acid residues, thus, it is used to monitor the tertiary structural disruption of the enzyme in the presence of inactivator. Our results showed that increase Al^{3+} concentration caused the Mn-SOD ANS-fluorescence intensity increase in a concentration-dependent manner.

3.4. Computational Docking Simulation for Mn-SOD and Al^{3+}. Because the crystallographic structure of Mn-SOD from *Thermus thermophilus* has been elucidated (PDB ID: 3MDS), we easily constructed the 3D structure of Mn-SOD. The docking between Mn-SOD and Al^{3+} by using Dock6.3 was successful with significant score (−14.07 kcal/mol) and we searched for Al^{3+} binding residues of Mn-SOD. We found that the most important expected binding residues interacting with Al^{3+} were ASP152 and GLU157 residues (box in Figure 8). The docking simulation provided the supportive information for the inactivation of Mn-SOD by Al^{3+} where the binding site is not located in the manganese-containing active site pocket (Figure 9). We found that Al^{3+}-induced inactivation of Mn-SOD is not due to the replacement of manganese or chelating from the active site.

4. Discussion

Several biological effects of Al^{3+} have been reported [12–15]: the results were mostly focused on the toxic effects such as the involvement of oxidative stress, deregulation of cell signaling,

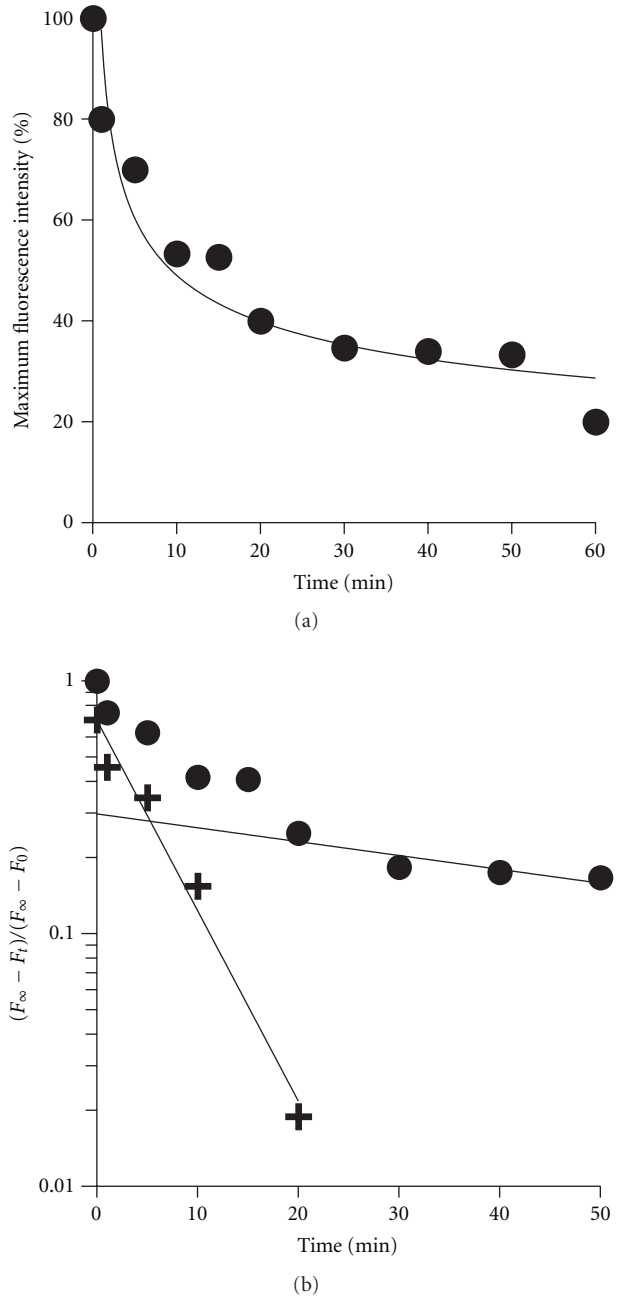

Figure 6: The kinetics of Al^{3+}-induced fluorescence spectra changes. (a) Plot of maximum intensity versus time (min). Intrinsic fluorescence spectra changes were measured in response to 0.2 mM Al^{3+} for various time intervals. The final Mn-SOD concentration was 1.6 μM. (b) A semilogarithmic plot. (•) Experimental points. (+) Points obtained by subtracting the contribution of the slow phase from the data in the curve (- - -). F_t: maximum intensity at various time interval; F_∞: maximum intensity at equilibrated state; F_0: maximum intensity at initial state.

membrane biophysics alterations, and the neurotoxicity in neurotransmission. On the contrary, a study reported that Al^{3+} can promote faster wound healing in response to skin injury [16] when it is prepared as the template to generate large uniform membranes with differing nanopore sizes.

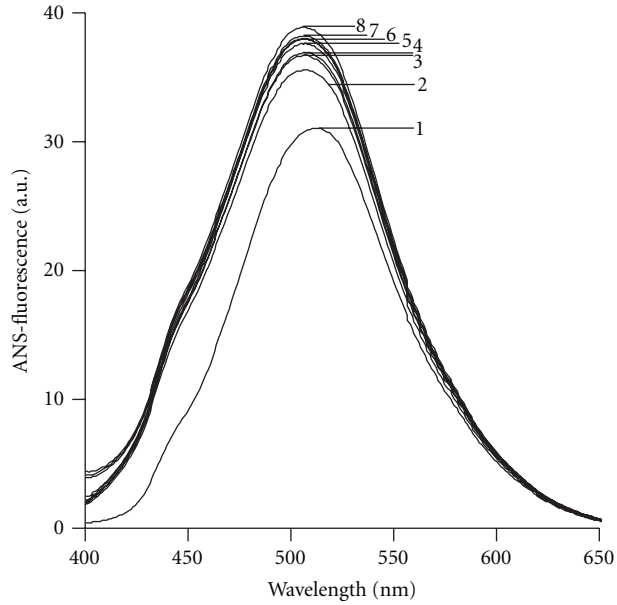

Figure 7: The ANS-binding fluorescence changes of Mn-SOD by Al^{3+}. ANS-binding fluorescence spectra in the presence of various concentrations of Al^{3+}. ANS (40 μM) was incubated for 30 min to label the hydrophobic surface of Mn-SOD prior to measurement. Other conditions were as for Figure 4. Curves from 1 to 8 indicate in 0, 0.01, 0.05, 0.1, 0.2, 0.3, 0.4, and 0.5 Al^{3+} mM, respectively.

Our investigation suggested a possible cytotoxic effect of Al^{3+} induced by Mn-SOD inhibition and it may sequentially induce the oxidative damage. Our data consistently supports the previous report that Al^{3+} acted as a toxic material for skin fibroblasts [17].

The changes of enzyme activity and structure in various ions have been extensively studied. For the case of Al^{3+}, it has been applied to several enzymes [18–20] to test its effects on the activities. The biological effect of Al^{3+} has been gradually elucidated and in this regard, we mainly focused on the changes in Mn-SOD activity and structures in Al^{3+} solutions in the present study, and we found that Al^{3+} worked as an inactivator to Mn-SOD accompanying with kinetic unfolding processes both in activity and structures. The relative activity and the conformational changes were synchronized in overall concentration of Al^{3+}. The activity of Mn-SOD was conspicuously observed when the secondary structure change has not yet occurred. The tertiary structural change of Mn-SOD by Al^{3+} was confirmed by the result of exposing the hydrophobic surface. Even at low concentration of Al^{3+}, the overall structure of Mn-SOD was changed and this directly affected the structural shape of active site pocket, regardless of Mn-SOD active center site is very impact and stable due to manganese contained inside. Al^{3+} binding site is distinctive to the substrate binding site of Mn-SOD. Al^{3+} did not directly compete with substrate but it affect the catalysis with a dose-dependent manner, implying that Al^{3+} binding site is near to substrate docking site. The computational simulations supported this observation that Al^{3+} can form a ligand-binding complex directly with ASP152 and GLU157 residues of Mn-SOD, and these amino acid residues are

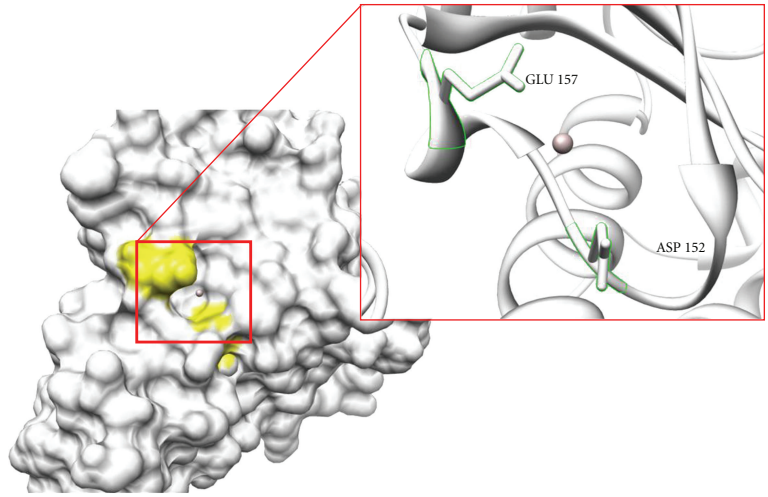

Figure 8: Computational docking simulations between Mn-SOD and Al^{3+}. 3D structure of Mn-SOD was constructed from PDB (ID: 3MDS), and the red box indicates the predicted binding sites for Al^{3+} via Dock6.3. Right red box shows the Al^{3+} binding residues.

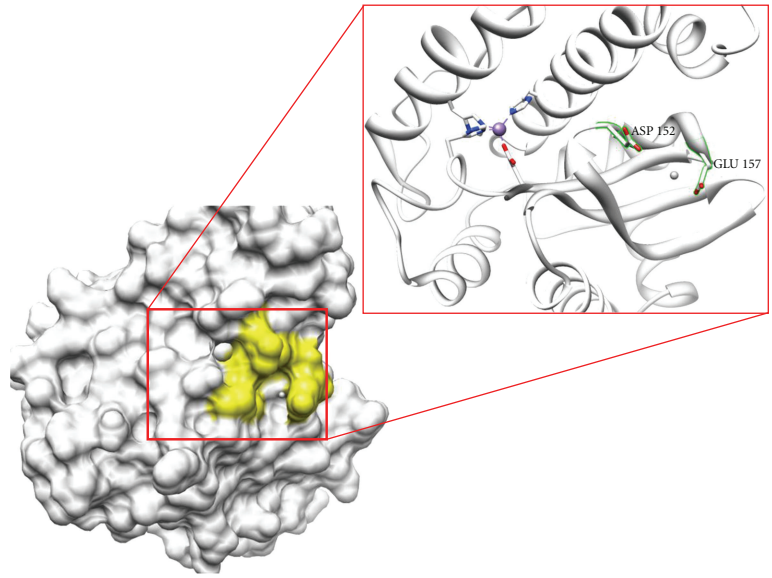

Figure 9: A comparison of active site and Al^{3+} docking site. Left part shows active site containing manganese metal (gray ball) and right part indicates Al^{3+} binding site.

not located in the active site. Therefore, the conformational changes were observed firstly prior to the occurrence of activity loss since the active site is relative compact and stable via manganese presence and Al^{3+} docking site is relative flexible part of Mn-SOD.

According to the results observed in the present study, we deduced the mechanisms of Mn-SOD response to Al^{3+}: (i) Al^{3+} ligand-binding to Mn-SOD causes fist-order kinetic inactivation which was synchronized with conformational changes; (ii) Al^{3+} also induced the decrease of secondary structure at relatively high concentration but compared to the activity and tertiary structural changes, the secondary structure was less sensitive to Al^{3+} than the tertiary structure; (iii) interestingly, the result of computational simulation support our supposition that Mn-SOD was bound to the near of active site, not in the inner site of active site pocket.

In conclusion, Mn-SOD from extremophile such as *Thermus thermophilus* was tend to be very stable against the changes of temperature and pH, as well as denaturants addition such as urea and guanidine hydrochloride. However, we found that Mn-SOD from *Thermus thermophilus* was conspicuously denatured by Al^{3+}. Taken together, the inhibition kinetics combined with the computational prediction allowed us to elucidate into the relationship between enzymatic reaction and structural changes of Mn-SOD from *Thermus thermophilus* and provides greater insight regarding the folding of Mn-SOD as well as the cytotoxicity of Al^{3+}.

Conflict of Interests

There is no conflict of interests in this study.

List of Abbreviations

Mn-SOD: Manganese-containing superoxide dismutase SOD
ANS: 1-anilinonaphthalene-8-sulfonate.

Acknowledgments

This work was supported by grants of Key Science and Technology Innovation Teams of Zhejiang Province (Grants no. 2009R50031 and no. 2009R50031-1) from the Science and Technology Department of Zhejiang Province, and the Zhejiang Provincial Top Key Discipline of Modern Microbiology and Application (Grants no. KF2010006 and no. KF2010007). Dr. Hae Young Chung was supported by National Research Foundation of Korea (NRF) Grant funded by the Korea Government (MOST) (no. 20090083538).

References

[1] A. K. Holley, S. K. Dhar, and D. K.S. Clair, "Manganese superoxide dismutase versus p53: the mitochondrial center," *Annals of the New York Academy of Sciences*, vol. 1201, pp. 72–78, 2010.

[2] L. Miao and D. St. Clair, "Regulation of superoxide dismutase genes: implications in disease," *Free Radical Biology and Medicine*, vol. 47, no. 4, pp. 344–356, 2009.

[3] C. L. Fattman, L. M. Schaefer, and T. D. Oury, "Extracellular superoxide dismutase in biology and medicine," *Free Radical Biology and Medicine*, vol. 35, no. 3, pp. 236–256, 2003.

[4] Y. Niwa, "Lipid peroxides and superoxide dismutase (SOD) induction in skin inflammatory diseases, and treatment with SOD preparations," *Dermatologica*, vol. 179, supplement 1, pp. 101–106, 1989.

[5] P. V. Sravani, N. K. Babu, K. V. T. Gopal et al., "Determination of oxidative stress in vitiligo by measuring superoxide dismutase and catalase levels in vitiliginous and non-vitiliginous skin," *Indian Journal of Dermatology, Venereology and Leprology*, vol. 75, no. 3, pp. 268–271, 2009.

[6] G. Raho, N. Cassano, V. D'Argento, G. A. Vena, and F. Zanotti, "Over-expression of mn-superoxide dismutase as a marker of oxidative stress in lesional skin of chronic idiopathic urticaria," *Clinical and Experimental Dermatology*, vol. 28, no. 3, pp. 318–320, 2003.

[7] Y. Zhao, Y. Xue, T. D. Oberley et al., "Overexpression of manganese superoxide dismutase suppresses tumor formation by modulation of activator protein-1 signaling in a multistage skin carcinogenesis model," *Cancer Research*, vol. 61, no. 16, pp. 6082–6088, 2001.

[8] Y. Zhao, T. D. Oberley, L. Chaiswing et al., "Manganese superoxide dismutase deficiency enhances cell turnover via tumor promoter-induced alterations in AP-1 and p53-mediated pathways in a skin cancer model," *Oncogene*, vol. 21, no. 24, pp. 3836–3846, 2002.

[9] S. Marklund and G. Marklund, "Involvement of the superoxide anion radical in the autoxidation of pyrogallol and a convenient assay for superoxide dismutase," *European Journal of Biochemistry*, vol. 47, no. 3, pp. 469–474, 1974.

[10] M. X. Xie, X. Y. Xu, and Y. D. Wang, "Interaction between hesperetin and human serum albumin revealed by spectroscopic methods," *Biochimica et Biophysica Acta*, vol. 1724, no. 1-2, pp. 215–224, 2005.

[11] D. T. Moustakas, P. T. Lang, S. Pegg et al., "Development and validation of a modular, extensible docking program: DOCK 5," *Journal of Computer-Aided Molecular Design*, vol. 20, no. 10-11, pp. 601–619, 2006.

[12] V. Kumar and K. D. Gill, "Aluminium neurotoxicity: neurobehavioural and oxidative aspects," *Archives of Toxicology*, vol. 83, no. 11, pp. 965–978, 2009.

[13] S. V. Verstraeten, L. Aimo, and P. I. Oteiza, "Aluminium and lead: molecular mechanisms of brain toxicity," *Archives of Toxicology*, vol. 82, no. 11, pp. 789–802, 2008.

[14] D. Krewski, R. A. Yokel, E. Nieboer et al., "Human health risk assessment for aluminium, aluminium oxide, and aluminium hydroxide," *Journal of Toxicology and Environmental Health. Part B*, vol. 10, supplement 1, pp. 1–269, 2007.

[15] P. P. Gonçalves and V. S. Silva, "Does neurotransmission impairment accompany aluminium neurotoxicity?" *Journal of Inorganic Biochemistry*, vol. 101, no. 9, pp. 1291–1338, 2007.

[16] L. G. Parkinson, N. L. Giles, K. F. Adcroft, M. W. Fear, F. M. Wood, and G. E. Poinern, "The potential of nanoporous anodic aluminium oxide membranes to influence skin wound repair," *Tissue Engineering. Part A*, vol. 15, no. 12, pp. 3753–3763, 2009.

[17] R. Anane, "Lipid peroxidation as pathway of aluminium cytotoxicity in human skin fibroblast cultures: prevention by superoxide dismutase+catalase and vitamins E and C," *Human and Experimental Toxicology*, vol. 20, no. 9, pp. 477–481, 2001.

[18] S. Kumar, "Biphasic effect of aluminium on cholinergic enzyme of rat brain," *Neuroscience Letters*, vol. 248, no. 2, pp. 121–123, 1998.

[19] M. I. Yousef, "Aluminium-induced changes in hematobiochemical parameters, lipid peroxidation and enzyme activities of male rabbits: protective role of ascorbic acid," *Toxicology*, vol. 199, no. 1, pp. 47–57, 2004.

[20] D. Orihuela, V. Meichtry, N. Pregi, and M. Pizarro, "Short-term oral exposure to aluminium decreases glutathione intestinal levels and changes enzyme activities involved in its metabolism," *Journal of Inorganic Biochemistry*, vol. 99, no. 9, pp. 1871–1878, 2005.